

STUDY OF SECONDARY ELECTRONS AND POSITRONS PRODUCED BY TERRESTRIAL GAMMA-RAY FLASHES

D. Sarria¹, P.-L. Blelly¹, and F. Forme¹,

Abstract. Terrestrial Gamma ray Flashes are emissions of X and gamma rays, correlated to thunderstorms. By interacting with the atmosphere, the photons produce a large number of electrons and positrons. Some of these reach altitudes above ~ 100 km that their interactions with the atmosphere become negligible, and they are then guided by Earth's magnetic field lines, forming the so called Terrestrial Electron Beams. The GBM instrument of the Fermi Space Telescope made a particularly interesting measurement of such an event that happened the 12/09/2009.

We perform Monte-Carlo simulations to study this event in detail and we focus on the resulting time histograms. In agreement with previous works, we show that the histogram measured by Fermi GBM can be reproduced from simulations. We then show that the time histogram can be decomposed into three populations of leptons, coming from the hemisphere opposite from the TGF, and mirroring back to the satellite with interactions with the atmosphere or not, and that these we can be clearly distinguished both with their pitch angles.

Keywords: TARANIS, XGRE, IDEE, TGF, Terrestrial gamma ray flash, relativistic, electrons, TEB, pitch angles, gamma rays, x rays, photons

1 Introduction

Terrestrial Gamma Ray flashes (TGF) are bursts of X and gamma photons associated with lightning, and detected mostly from space. TGFs were first presented by Fishman et al. (1994), using data from the BATSE experiment on-board the CGRO spacecraft. Later, TGF were detected from space by RHESSI (Smith et al. 2005), AGILE (Marisaldi et al. 2014) and Fermi (Briggs et al. 2010). TARANIS (XGRE and IDEE instruments) (Lefevre et al. 2009) from CNES and ASIM (MXGS instrument) from ESA are planned for the next years and will be dedicated to the study of TGF and secondary electron emissions.

A comprehensive review of the high energy emissions associated with lightning is presented in Dwyer et al. (2012). The production mechanism of TGFs may be explained by the cold runaway model (Moss et al. 2006; Celestin et al. 2012; Chanrion et al. 2014) or the relativistic feedback model (Dwyer 2012). Observations of TGFs from space, together with their associations with radio emissions from ground, allowed to constrain some important properties (Dwyer & Smith 2005; Cummer et al. 2014). They present :

- A bremsstrahlung type energy spectrum with a maximum energy of about 30 MeV
- A duration between 10 μ s and 0.5 ms.
- An emission altitude located between 10 and 20 km (inside or immediately above thunderclouds)
- A fluence of ~ 1 photon/cm² at about 500 km altitude, which requires to have at least 10¹⁶ high energy photons at the source.

Once produced, these primary photons from the TGF interact with the atmosphere. As a result of these interactions, secondary electrons and positrons are produced, and a part of these particles can reach an altitude where they stop interacting significantly with the atmosphere. Their motion is then guided by the geomagnetic

¹ CNRS, IRAP, 9 Av. colonel Roche, BP 44346, F-31028 Toulouse cedex 4, France.

field, forming the so-called Terrestrial Electron Beams (TEBs) (Dwyer et al. 2008). Following field lines, TEBs can travel from an hemisphere to another, and can lead to "false TGF" detections (since they are due to electrons and not to X/gamma-rays), like the anomalous RHESSI TGF event (Smith et al. 2006) detected above a desert. Such events are significantly longer than TGFs, with a typical duration > 1 ms. In some cases, due to the conservation of the first adiabatic invariant, a part of the electrons can mirror and go back to the satellite, leaving a specific signature of a dual pulse in the satellite measurement. Such events could be found in BATSE's data (Dwyer et al. 2008) and later with Fermi GBM, particularly with the 091214 event (Briggs et al. 2011). This event has 1735 counts, about four times more than the other TEB events recorded, making it a perfect candidate for simulations.

For this study, we performed Monte-Carlo simulations, using the MC-PEPTITA Monte-Carlo model, presented into detail in (Sarria et al. 2015). First, we discuss the initial conditions of the simulations to define a "standard" TGF. Then we compare with simulations the TEB lightcurve detected by Fermi GBM, and show how it can be decomposed by looking at the pitch angles of the electrons and positrons.

2 Initial conditions

A simulation is started with a given number of photons N_p . As written before, in a real TGF, in order to have about 1 photon/cm² at satellite altitude, it is estimated that 10^{16} high energy photons have to be produced at the source. This quantity is not reachable in a reasonable amount of time. We present here simulations with $N_p = 10^8$, high enough to build the distributions with we need low noise. The altitude where the TGF's Bremsstrahlung photons are produced is supposed to be $h = 15$ km, and the latitude (λ) and longitude (ϕ) are set to -13.0° and $\phi = 32.0^\circ$. Following Carlson et al. (2011), the angle distribution of the photon beam is assumed to follow a normal distribution that has a σ_θ parameter set to 35° . Let E be the energy of a TGF photon. We set a standard TGF spectrum with an energy distribution function $P(E) \propto 1/E \exp(-E/\epsilon)$, where ϵ is the cut-off energy, set to 7.3 MeV. This spectrum is reasonably close to the exact spectrum (Dwyer et al. 2012). The minimum energy is set to 10 keV and the upper limit is set to 30 MeV.

The Relativistic Feedback Discharge Model (RFD) (Dwyer 2012) gives time distributions of the primary photons that are symmetrical (the rise time is close to the fall time) for all pulse duration. We make the assumption that it is a normal distribution, with a standard deviation parameter σ_{TGF} . A value of 0.15 ms fits the typical TGF lightcurve shown in Dwyer (2012).

In the simulations, the status (energy, position, velocity, ...) of each lepton is saved when it crosses 565 km altitude, downward or upward. In the example of the Fermi 091214 event, the simulation shows that the center of the electron beam crosses the satellite altitude at two positions: ($\lambda = -8.46^\circ, \phi = 31.7^\circ$) and ($\lambda = 25.5^\circ, \phi = 31.4^\circ$). The second value is close to the actual position of Fermi ($\lambda = 25.34^\circ, \phi = 31.42^\circ$). All the leptons distributions that are discussed hereafter are built considering only the particles in the northern hemisphere, with a radial distance lower than 50 km from the center of the beam.

3 Results

3.1 Basic comparison

Figure 1 shows the time distribution of the electrons and positrons reaching the satellite altitude. We compare the simulated data (blue curve for electrons, green curve for positrons) with the measurement made by Fermi GBM (shown as a the black curve).

A simple model using only three parameters (a time shift $t_s = -19.2$ ms, a scale factor $A = 1/62.9$, and a constant background rate $b = 9$ counts per 0.5 ms) is applied for the simulated time histograms to match the Fermi lightcurve. The two histograms fit very accurately, with a coefficient of determination $r^2 = 0.92$. This is similar to the result of the simulation done by Dwyer et al., presented in (Briggs et al. 2011), and reproduced in figure 1 (magenta curve). This confirms independently that this time histogram is due to electrons that are coming to the satellite from the southern hemisphere (first pulse between 0 ms and 12 ms) with a part that is then bouncing on a magnetic mirror point and reaching the satellite a second time (second pulse between 21 and 27 ms). The positron histogram is similar to the electron histogram, with a scale factor of $A_p = 8$.

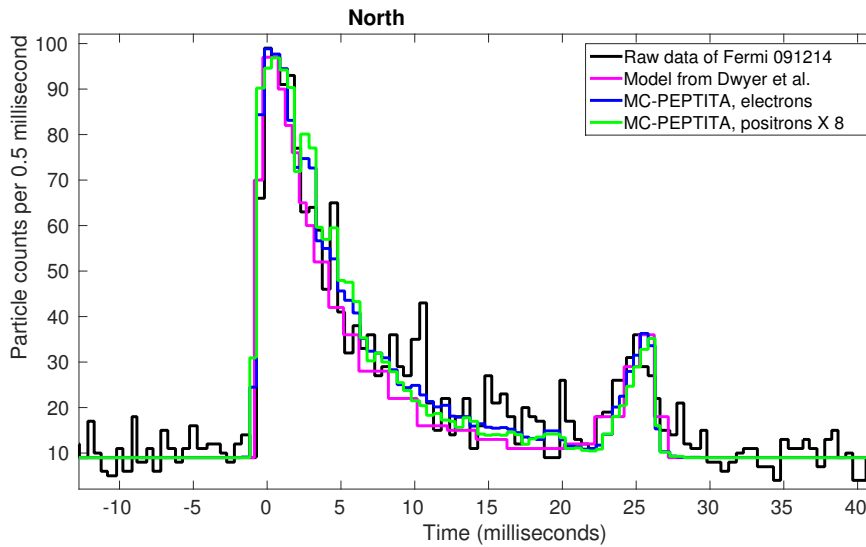


Fig. 1. Time histogram of the Fermi event 091214. Comparison between the Fermi GBM data, the simulations of Dwyer et al. for electrons (both extracted from Briggs et al. (2011)) and MC-PEPTITA simulations (for electrons and positron). The positron histogram is scaled by 8.

3.2 Pitch angle decomposition

Let v be the magnitude of the velocity vector of a lepton, which is constant when the lepton is not interacting with the atmosphere, because of conservation of energy (only the Earth's magnetic field is applied on the particle). Let v_{\parallel} be the part parallel to its local geomagnetic field. The pitch angle α of a lepton is defined as the angle between its velocity vector and the local magnetic field direction. Figure 2.a. and 2.b. show the lightcurve of leptons crossing satellite altitude (~ 550 km) in the northern hemisphere. We are using the same definitions of the normal and log-normal distributions that are presented in (Briggs et al. 2010), as well as a Poisson log-likelihood minimization as a method to find the best fits.

Figure 2.a. shows the lightcurve of the leptons that are coming from the southern hemisphere, meaning they have α values between 0° and 90° . The lightcurve of the leptons of figure 2.a. is well fit by a log-normal distribution (red) : it has a coefficient of determination $r^2 = 0.99$. This log-normal time distribution is due to differences in time delays due to differences of pitch angles α of the leptons once they escape the atmosphere. Actually, all the leptons will follow very similar magnetic field lines, but the ones with the lowest pitch angles when escaping will have the highest v_{\parallel} (still in the case where $\alpha < 90^{\circ}$). The two quantities are linked with $v_{\parallel} = v \cos(\alpha)$. α increases along the trajectory of the lepton due to conservation of the first adiabatic invariant. At satellite altitude, the value of v is $\approx 0.98 c$ on average and the value of v_{\parallel} is $\approx 0.5 c$ on average.

The time distribution of figure 2.b. can be split into two parts. From about 5 to 21 ms, we see that the distribution can be very well fit using a gaussian (normal) function. The population located from about 21 to 27 ms can be well fit by a mirrored log-normal function. This model fits well the data since its overall coefficient of determination is $r^2 = 0.98$. The two sub-populations of electrons/positrons can be easily separated with their pitch angles, as shown by figure 2.c. There is a clear difference between the leptons above and below $\alpha \approx 120^{\circ}$. Actually, a pitch angle of about 120° at this position ($h = 565$ km, $\lambda = 25.5^{\circ}$, $\phi = 31.4^{\circ}$) corresponds to electrons that had a mirroring altitude of ~ 100 km, the altitude above which the interactions with the atmosphere occur so infrequently that they are negligible. Therefore, we define 100 km as the limit of the atmosphere in this context. Below $\approx 120^{\circ}$, the distribution is weakly spread, and corresponds to the leptons that had a pitch angle between $\approx 60^{\circ}$ and 90° and came back to satellite's altitude after mirroring, without interacting with the atmosphere. Indeed, figure 2.c. shows that the number of leptons between 60° and 90° is similar to the number between 90° and $\approx 120^{\circ}$, each representing $\approx 11\%$ of the total count. We also know it because the particles are tagged. All the leptons that are coming to the satellite with pitch angles below $\approx 60^{\circ}$ were inside the loss cone (the range of angles where the particles have mirroring altitudes inside the atmosphere), but not all of them are absorbed. $\approx 8\%$ of the total count can mirror back to satellite altitude. These leptons interacted weakly enough with the atmosphere, but strongly enough to be scattered back outside

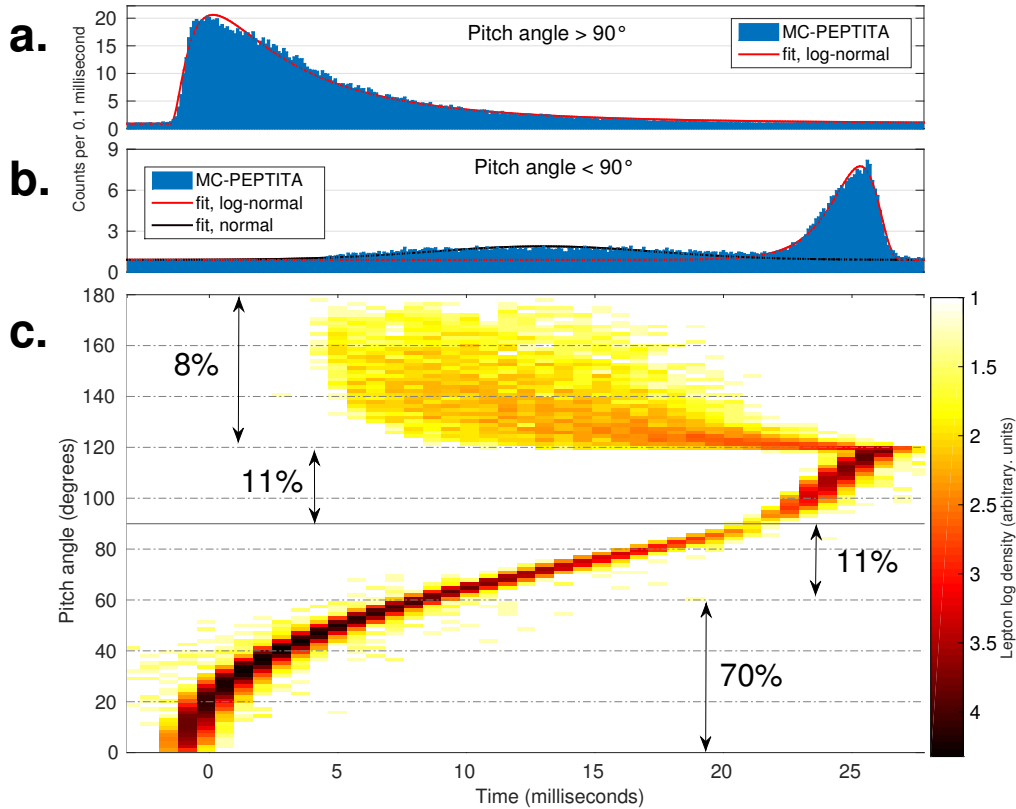


Fig. 2. Time and pitch angles distributions for leptons crossing the altitude of the satellite. The time scale (x-axis) is shared by the three plots. Electrons and positrons coming to the satellite from the southern hemisphere will have a pitch angle α between 0° and 90° , whereas leptons coming back to the satellite after mirroring will have pitch angles between 90° and 180° . **a.** Simulated time histogram, only for leptons with pitch angles $> 90^\circ$. The red curve is a log-normal fit. **b.** Simulated time histogram, only for electrons and positrons with pitch angles $< 90^\circ$. The red curve is a log-normal fit, the black curve is a normal fit. **c.** Density distribution of pitch angle and time. The fractions of the total number of leptons included inside pitch angle ranges are also given.

the atmosphere. Random interactions with the atmosphere result in random time delays, resulting to a time distribution, seen at satellite altitude, with approximately a normal shape.

4 Conclusions

We performed MC-PEPTITA simulations of the Fermi 091214 TGF/TEB event, supposing an initial TGF formed by a photons source, defined with reasonable parameters for its position, energy spectrum, beaming, and time distribution. The lightcurve detected by Fermi is shown to be accurately reproducible from simulations, in agreement with previous work.

Furthermore, we showed that this lightcurve can be decomposed into three components. The first, coming directly from the hemisphere where the TGF was originally emitted, has pitch angles ranging between 0° and 90° with a log-normal time distribution. Leptons coming back to the satellite altitude after mirroring have pitch angles between 90° and 180° , and can be decomposed into two components : the leptons that have interacted significantly with the atmosphere and the leptons that did not. If they did, their pitch angles range between $\approx 120^\circ$ and 180° , and their lightcurve can be well fit by a normal distribution. If they did not, their pitch angles range between 90° and $\approx 120^\circ$ and their time distribution can be well fit by a mirrored log-normal function.

The TARANIS satellite, with the XGRE and IDEE instrument, will have the ability to measure the lightcurves and pitch angle distribution of the electrons, and should provide reliable information about these properties.

We would like to thank the "Centre National d'Etudes Spatiales" (CNES), and the "Direction Generale de l'Armement" (DGA) for their support.

This work was granted access to the HPC resources of CALMIP supercomputing center under the allocation 2015-p1505.

References

- Briggs, M. S., Connaughton, V., Wilson-Hodge, C., et al. 2011, *Geophys. Res. Lett.*, 38, 2808
- Briggs, M. S., Fishman, G. J., Connaughton, V., et al. 2010, *Journal of Geophysical Research (Space Physics)*, 115, 7323
- Carlson, B. E., Gjesteland, T., & Østgaard, N. 2011, *Journal of Geophysical Research (Space Physics)*, 116, 11217
- Celestin, S., Xu, W., & Pasko, V. P. 2012, *Journal of Geophysical Research (Space Physics)*, 117, 5315
- Chanrion, O., Bonaventura, Z., Çinar, D., Bourdon, A., & Neubert, T. 2014, *Environmental Research Letters*, 9, 055003
- Cummer, S. A., Briggs, M. S., Dwyer, J. R., et al. 2014, *Geophysical Research Letters*, n/a
- Dwyer, J. R. 2012, *Journal of Geophysical Research (Space Physics)*, 117, 2308
- Dwyer, J. R., Grefenstette, B. W., & Smith, D. M. 2008, *Geophysical Research Letters*, 35, n/a
- Dwyer, J. R. & Smith, D. M. 2005, *Geophys. Res. Lett.*, 32, 22804
- Dwyer, J. R., Smith, D. M., & Cummer, S. A. 2012, *ssr*, 173, 133
- Fishman, G. J., Bhat, P. N., Mallozzi, R., et al. 1994, *Science*, 264, 1313
- Lefevre, F., Blanc, E., & Pinçon, J. L. 2009, in *American Institute of Physics Conference Series*, Vol. 1118, American Institute of Physics Conference Series, 3–7
- Marisaldi, M., Fuschino, F., Pittori, C., et al. 2014, in *EGU General Assembly Conference Abstracts*, Vol. 16, EGU General Assembly Conference Abstracts, 11326
- Moss, G. D., Pasko, V. P., Liu, N., & Veronis, G. 2006, *Journal of Geophysical Research (Space Physics)*, 111, 2307
- Sarria, D., Blelly, P.-L., & Forme, F. 2015, *Journal of Geophysical Research: Space Physics*, n/a, 2014JA020695
- Smith, D. M., Grefenstette, B. W., Splitt, M., et al. 2006, *AGU Fall Meeting Abstracts*, A1040
- Smith, D. M., Lopez, L. I., Lin, R. P., & Barrington-Leigh, C. P. 2005, *Science*, 307, 1085